Journal of Marine Science and Technology

Volume 26 | Issue 5 Article 1

AN EXPERIMENTAL AND NUMERICAL STUDY OF A HIGH SPEED PLANING CRAFT WITH FULL-SCALE VALIDATION

Ahmet Gultekin Avci
Istanbul Technical University, Faculty of Naval Arch & Ocean Engineering, Istanbul, Turkey, g.avci@itu.edu.tr

Baris Barlas
Istanbul Technical University, Faculty of Naval Arch & Ocean Engineering, Istanbul, Turkey.

DOI: 10.6119/JMST.201810_26(5).0001
Available at: https://jmstt.ntou.edu.tw/journal/vol26/iss5/1

AN EXPERIMENTAL AND NUMERICAL STUDY OF A HIGH SPEED PLANING CRAFT WITH FULL-SCALE VALIDATION

Acknowledgements

The authors would like to thank the staff of Ata Nutku Ship Model Testing Laboratory at Istanbul Technical University for their assistance during the experiments and Istanbul Technical University Scientific Research Projects Support Program for partial support of this research through the project ITU-BAP38875. The authors also would like to thank “Loça Mühendislik” Ship Design Company for their support and for access to the full-scale trial data.

Journal of Marine Science and Technology, Vol. 26, No. 5, pp. 617-628 (2018)
DOI: 10.6119/JMST.201810_26(5).0001

AN EXPERIMENTAL AND NUMERICAL STUDY OF A HIGH SPEED PLANING CRAFT WITH FULL-SCALE VALIDATION

Ahmet Gultekin Avci and Baris Barlas

Key words: high speed crafts, resistance, full-scale, ship model test.

ABSTRACT

During the conceptual design of a high speed craft, the most important element of the process is resistance and drag prediction. To increase efficiency in high speed craft design, the prediction of total resistance must be increasingly accurate. To achieve this objective, model towing tank tests were used. Although testing will always be necessary, the growing field of computational fluid dynamics (CFD) is gaining interest, considering the experimental costs. This paper investigates both the experimental and numerical methods of total resistance prediction for a high speed hull, including comparison of the trim and sinkage measurements. Additionally, the model tests were compared to CFD methods when considering the numerical ventilation problem (NVP) and were also validated with full-scale test results. It was shown that at high speeds, the numerical solution of the ventilation problem may lead to an erroneous drag reduction of 27%. To overcome this, replacing the air phase with the water phase under the hull provides an efficient solution. For the numerical solutions with Froude number (Fn) > 0.50 after resolving the NVP, the calculated total resistance shows quite good agreement with the experimental data, with a margin of 2.86%.

I. INTRODUCTION

Although the number of investigations has dramatically increased, there is an overwhelming need to study the design of an efficient high speed craft. In recent years, motorboats, pilot boats, personnel carriers, search and rescue (SAR) boats and some passenger boats have all been considered for attaining high speeds. Accelerating to a high speed is directly related with resistance characteristics and hull form. At high speeds, the hull is subjected to dynamic effects, because of the hydrodynamic characteristics of the geometry, as well as the heave and pitch motions, termed trim and sinkage. At high speeds, according to the dynamic conditions of the rigid body, the total resistance increases rapidly and leads to excessive fuel consumption. Generally, with Froude numbers between 0.4 and 0.6, a typical high speed craft enters the transient (hump) regime. After the transient regime, the rate of increase in total drag on the hull is slower than that of semi-planing hulls or other semi-displacement hulls. As the vessel advances through higher speeds, the wave resistance also increases. To estimate the total resistance of the full scale ship, in addition to the drag values, all attitudes including trim and sinkage must be considered and predicted accurately.

The planing hulls moving at high speed also generate hydrodynamic lift, which reduces the wave-making resistance and may generate spray around the bow zone. The spray should also be considered and visualized in the early stages of ship design, because it is intricately tied to the geometry, trim and speed of the hull. For the most accurate results, high speed craft model tests have been the industry standard for decades. Model tests estimate total resistance characteristics of a high speed boat, but trim and sinkage values must also be measured correctly to be included in full-scale analyses.

An extensive database was created by Clement and Blount (1963) encompassing model experiment results, including the drag measurements of the TMB Series 62 (the Clement Series) model. On the hydrodynamic design of planing hulls, Savitsky (1964) has led studies in this growing field of interest and has formulated simple procedures. Faltinsen (2006) concluded that the main forces balancing the weight of the hull are the buoyancy and the hydrodynamic lift, both for planing and semi-planing modes. Ghassemi and Ghiasi (2008) presented a combined technique, consisting of a potential-based boundary element method and boundary layer theory to calculate the hydrodynamic induced resistance and lift coefficient of planing crafts. Brizzolara and Serra (2011) investigated the flow around the high speed planing hulls using finite volume method. Kim et al. (2013) studied the design of high speed planing hulls for improved resistance and seakeeping performance, declaring that high speed marine vehicles must have optimal resistance characteristics for

Paper submitted 08/29/17; revised 02/26/18; accepted 06/07/18. Author for correspondence: Ahmet Gultekin AVCI (e-mail: g.avci@itu.edu.tr).
[1] Istanbul Technical University, Faculty of Naval Arch & Ocean Engineering, Istanbul, Turkey.

safe operation in rough seas. They also acknowledged that high speed crafts are supported by buoyancy at low speeds, but require additional hydrodynamic lift at higher speeds. To accurately predict vertical displacement, accelerometers or other measurement devices are needed. Yousefi et al. (2013) improved hydrodynamic analysis techniques for high speed planing hulls. It was found that CFD methods were optimal, when analytical solutions of the governing equations were not possible. CFD methods have become more effective in addressing the limitations of model tests. Santoro et al. (2014) experimentally studied hydrodynamic loads on high speed planing crafts. The pressure distributions on the bottom of the hull were examined by measuring impact pressures for both time and frequency domains. Su et al. (2014) studied the numerical and experimental analyses of hydrodynamic performance of a channel type planing trimaran. A Reynolds-Averaged Navier Stokes Volume of Fluid (RANS-VOF) solver was used to evaluate the hydrodynamic performance of the hull and experiments were performed in a towing tank. Resistance characteristics were affected by the longitudinal center of the gravity. Mousaviraad et al. (2015) used Unsteady Reynolds-Averaged Navier Stokes (URANS) to compute the hydrodynamic performance and slamming loads on high speed planing hulls in calm water, in both deep and shallow water conditions. For simulations in calm water with free to trim and sinkage, a refined grid around the spray area was necessary for more accurate solutions. Stern et al. (2015) overviewed the importance of increased resolution for CFD analysis. Cerka et al. (2017) studied the numerical simulation of the research vessel hull form using traditional standard series analysis and CFD methods. The standard series analysis method was deemed not appropriate for the numerical simulations. Sukas et al. (2017) presented a study on the hydrodynamic assessment of planing hulls using overset grids, where a better approximation for complex fluid-structure interaction of the planing regime was found.

This paper investigates the experimental and numerical methods of resistance prediction of a high speed hull, including a comparison of the trim and sinkage measurements. Practical methods were also used for trim and sinkage measurements, using electronic devices such as an inertial measurement unit (IMU), a distance laser meter, a high speed camera system (HSCS) and low cost accelerometers. The model tests were compared to CFD methods, considering the numerical ventilation problem (NVP). Moreover, the model tests and CFD simulations were validated with the full-scale sea trial results.

II. EXPERIMENTAL PROCEDURE

The towing tank tests for the present study were carried out in Ata Nutku Ship Model Testing Laboratory at Istanbul Technical University. The tank dimensions were 160 m length, 6 m width and 4 m depth; for the tests within the water depth was set at 3.4 m. The carriage can accelerate up to 5 m/s with a high level of accuracy in speed control.

The wooden model of an 18.7 m length high-speed pilot boat was used in the towing tank for the desired loading conditions with a scale of 8.5, as shown in Fig. 1.

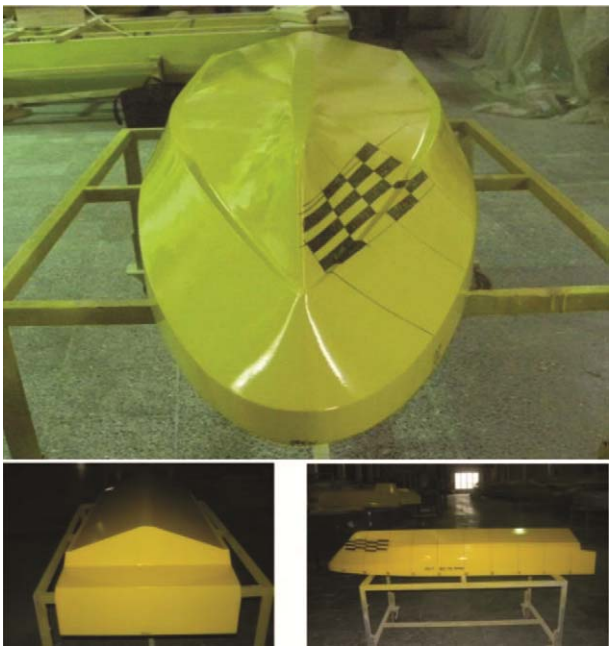

Fig. 1. Bow, aft and profile views of the wooden test model.

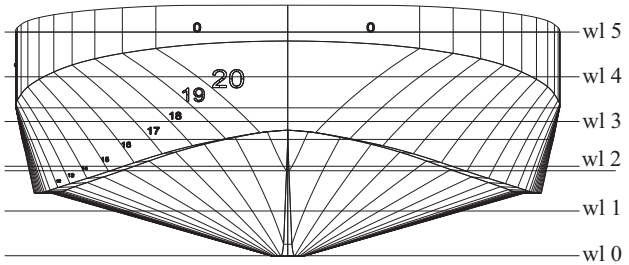

Fig. 2. Sectional curves of the model.

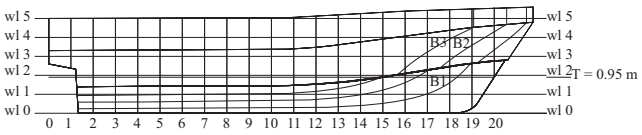

Fig. 3. Profile view of the model.

The geometric and hydrostatic details of the model and the high-speed pilot boat are given in Table 1. The sectional curves and the profile view of the boat are depicted in Fig. 2 and Fig. 3, respectively. The experimental setup photography is depicted in Fig. 4.

The model was tested over a speed range corresponding to 5-30 knots full scale. The experiment was conducted in accordance with the ITTC procedures (ITTC, 2008). The model was free to heave and pitch, and the towing point was located at the longitudinal center of gravity (LCG = LCB) without initial trim angles.

Table 1. The geometric and hydrostatic details of the model and the boat.

Test condition	Model (λ = 8.5)	Ship
Length between perpendiculars L_{BP} (m)	2.031	17.262
Length on waterline L_{WL} (m)	1.934	16.439
Wetted length L_{WS} (m)	1.934	16.439
Breadth B (m)	0.588	5.000
Draught (amidships) T (m)	0.109	0.918
Draught (AP) T_A (m)	0.108	0.918
Draught (FP) T_F (m)	0.108	0.918
Displacement volume ∇ (m^3)	0.053	32.750
Displacement Δ (ton)	0.053	33.569
Nominal wetted surface area S_0 (m^2)	0.989	71.520
Transom area A_T (m^2)	0.0256	1.855
Centre of transom area H_T (m)	0.0741	0.630
Block coefficient C_B	0.436	0.436
Prismatic coefficient C_P	0.715	0.715
Midship area coefficient C_M	0.611	0.611
Waterplane area coefficient C_{WP}	0.755	0.755
Longitudinal center of buoyancy LCB (m) fwd)	-0.128	-1.086
Longitudinal center of floatation LCF (m) (+fwd)	-0.130	-1.108
Service speed V_S	4.77 m/s	27.0 kts

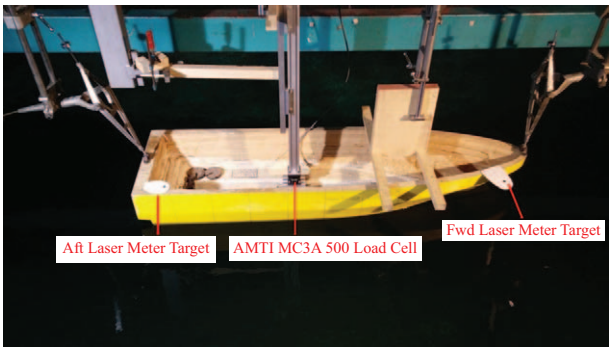

Fig. 4. Experimental setup of the towed model.

1. Drag Measurements

The ship was powered by water jet systems and no appendages were introduced. The drag force was measured by using AMTI's MC3A 500 load cell. Towing carriage speed was measured using an encoder mounted on a trailing wheel. All collected data was logged on to an HBM DAQ with a constant sampling rate of 100 Hz. Drag results were scaled up to full-scale using the ITTC 1978 procedure, and all results were corrected to a 15°C water temperature (ITTC, 2008).

2. Trim and Sinkage Measurements

There are numerous experiment systems for measuring heave and pitch motions of models in towing tanks, such as high-speed camera systems (HSCS), remote laser distance meters, linear variable differential transformers (LVDT) and inertial measurement units (IMU). According to the ITTC recommended procedures, sinkage fore and aft may be measured with mechanical guides, potentiometers, encoders, LDVTs or with remote (laser or ultrasonic) distance meters. The trim angle values were calculated from the measured running sinkage of fore and aft points during the model tests (ITTC, 2008).

III. MATHEMATICAL FORMULATION

1. Governing Equations

In the present study, to achieve realistic motions as visualized by the experiments, a rigid body motion with Dynamic Fluid Body Interaction (DFBI) model was used with two degrees of freedom (2DoF) to simulate trim and sinkage measurements. The equation for the translation of the center of mass of the model body, as used to calculate trim and sinkage values are given as;

$$M\frac{\partial}{\partial t}\omega = n \tag{1}$$

and

$$m\frac{dv}{dt} = f \tag{2}$$

where n is the resultant moment acting on the model according to the axis of rotation, M is the moment of inertia with respect to the rotation axis, ω is the angular velocity of rigid body with respect to the rotation axis, m represents the mass of the model,

f is the resultant force acting on the hull surface and v is the velocity of the center of mass. The resultant force and moment acting on the model were obtained from fluid pressure and shear force acting on each boundary face of the body. The translations of the model were estimated according to the calculated velocity and pressure fields in the flow domain. A detailed discussion of this topic can be found in the research by Panahani et al. (2009). The unsteady RANS equations for an incompressible, three-dimensional flow are the continuity equation:

$$\frac{\partial U_i}{\partial x_i} = 0 \tag{3}$$

and the momentum equation:

$$\frac{\partial U_i}{\partial t} + \frac{\partial \left(U_i U_j\right)}{\partial x_j} = -\frac{1}{\rho}\frac{\partial P}{\partial x_i} + \frac{\partial}{\partial x_j}\left[\nu\left(\frac{\partial U_i}{\partial x_j} + \frac{\partial U_j}{\partial x_i}\right)\right] - \frac{\partial \overline{u_i' u_j'}}{\partial x_j} \tag{4}$$

Here, x_i is the spatial coordinate, t is time, U_i is the mean velocity, u_i' is the fluctuating velocity, P is the mean pressure, ρ is the fluid density and v is the kinematic viscosity. The Reynolds stress tensor is modelled by the Boussinesq approximation:

$$\overline{u_i' u_j'} = v_t\left(\frac{\partial U_i}{\partial x_j} + \frac{\partial U_j}{\partial x_i}\right) + \frac{2}{3}\delta_{ij}k \tag{5}$$

The eddy viscosity based on the standard k-ε turbulence closure model was used. The eddy viscosity, v_t, is expressed as $v_t = C_\mu k^2/\varepsilon$, where C_μ is an empirical constant taken as 0.09, k is the turbulent kinetic energy and ε is the dissipation rate of k. The turbulence quantities, k and ε, were then calculated from the well-known standard k-ε turbulence model using two transport equations. The equations for turbulent kinetic energy, k, and the rate of dissipation of the turbulent energy, ε, can be given as;

$$\frac{\partial k}{\partial t} + \frac{\partial \left(kU_j\right)}{\partial x_j} = \frac{\partial}{\partial x_j}\left[\left(v + \frac{v_t}{\sigma_k}\right)\frac{\partial k}{\partial x_j}\right] + P_k - \varepsilon \tag{6}$$

$$\frac{\partial \varepsilon}{\partial t} + \frac{\partial \left(\varepsilon U_j\right)}{\partial x_j} = \frac{\partial}{\partial x_j}\left[\left(v + \frac{v_t}{\sigma_\varepsilon}\right)\frac{\partial \varepsilon}{\partial x_j}\right] + C_{\varepsilon 1}P_k\frac{\varepsilon}{k} - C_{\varepsilon 2}\frac{\varepsilon^2}{k} \tag{7}$$

Table 2. Mesh analysis.

Block	Block Name	Mesh Dimension
1	Far field	0.1454 L
2	Mid domain-1	0.0900 L
3	Mid domain-2	0.0727 L
4	Near model & free surface	0.0045 L
5	Free surface & model	0.0363 L

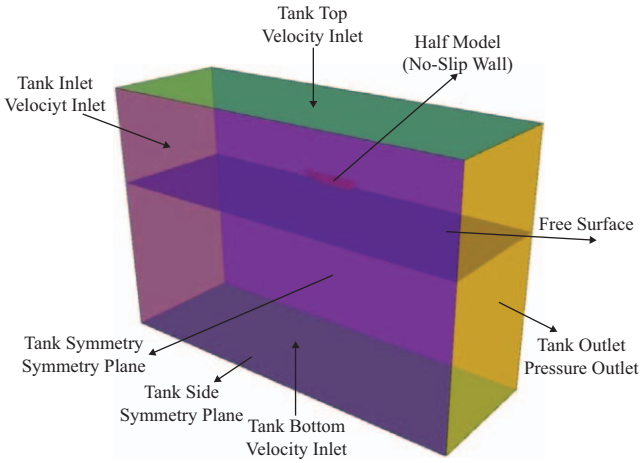

Fig. 5. Computational Domain of Towing Tank.

$$P_k = -\overline{u_i' u_j'}\frac{\partial U_i}{\partial x_j} \tag{8}$$

where, $C_{\varepsilon 1} = 1.44$, $C_{\varepsilon 2} = 1.92$ and the turbulent Prandtl numbers for k and ε are $\sigma_k = 1.0$, and $\sigma_\varepsilon = 1.3$. The pressure and velocity coupling problem is solved by using the semi-implicit method for pressure-linked equations (SIMPLE) algorithm, where the velocity field is first solved using a presumed pressure. The pressure and velocity fields are then corrected with the calculated values of pressure and velocity, as reported by Patankar and Spalding (2005). Calculations are made within an unstructured finite volume mesh for half of the model hull, symmetric about the longitudinal centerline.

2. Numerical Domain, Boundary Conditions and Mesh Generation

A half model approach was used to reduce the computational cost, such that a symmetry plane splits the domain down the centerline. The computational towing tank domain, with the model hull and the notations of the boundaries is shown in Fig. 5. The domain was taken to extend two model lengths fore of the model, three model lengths aft, two model lengths along the beam considering wave reflection and three model lengths in depth. A wave damping length was selected to avoid interaction between true and reflected waves. For the numerical simulations, the domain was discretized by using 4,607,090 grid points, with

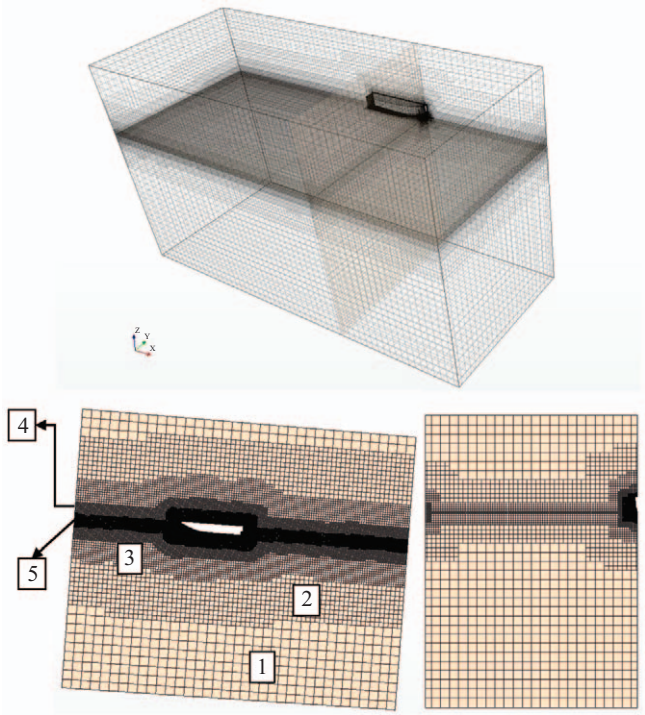

Fig. 6. The CAD geometry and mesh of the model.

the mesh concentrated near the hull and free surface. A trimmed cell mesher was employed to handle the complex mesh generation. Finite volume mesh was generated entirely with structured hexahedral cells as shown in Fig. 6, and the mesh analysis is given in Table 2. Within the far field, walls with slip boundary conditions were used.

At the model surface, walls with a no-slip condition and a zero gradient of velocity parallel to wall were specified, as the wall shear stress is zero under a free slip condition. At the tank outlet boundary, a zero derivative condition in x-direction was used, and pressure was hydrostatic. At the symmetry plane boundaries, a zero derivative condition in the normal directions was utilized.

Due to the well-mannered structure and well-established calculations, the standard k-ε turbulence model was preferred. Using the standard k-ε two-equation turbulence model, additional wall functions are essential to link solution variables between the wall and the fully-turbulent region. The velocity in the log-law region varies logarithmically with normalized wall distance y^+, as presented in Eq. (9) below. Although there are small differences in the values of universal constants within the literature, according to Stanford conventions, the Von Karman constant, $\kappa = 0.41$ and the constant $B = 5.0$, as reported by Dixit and Ramesh (2009).

$$U^+ = \frac{1}{\kappa}\ln\left(y^+\right) + B \tag{9}$$

where U^+ is the streamwise velocity non-dimensionalized by

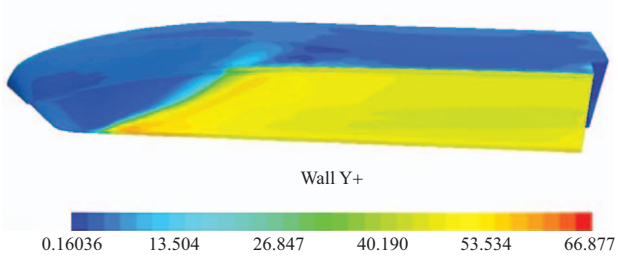

Fig. 7. Wall distance y^+ distribution around the model hull surface at Fn = 1.25.

the friction velocity u_τ. Fig. 7 depicts the normalized wall distance (y^+) distribution around the model hull surface at Fn = 1.25, after the solution has converged. The y^+ values on the model hull were calculated to be between 45 and 60, which is in agreement with the wall function application where the y^+ values are expected to be greater than 30.

IV. NUMERICAL METHOD

In this study, the numerical simulations of a planing type high speed marine vehicle in model scale were performed using the RANS-based commercial CFD software STAR-CCM+, which enables three dimensional VOF model simulations to capture the free surface between air and water. All simulations were carried out on 12 parallel clusters with 24 hyper-threading cores, allowing approximately 5 million cells. Results were obtained after four full days of running on the compute cluster. An Eulerian Multiphase model was needed for the free surface simulation, and it was created by using air and water phases with constant density and dynamic viscosity, matching the average temperature of the fresh water towing tank.

The governing equations were discretized using a node-based finite volume method. The advection terms were discretized using a first-order upwind interpolation scheme. The governing equations were solved consecutively. The numerical algorithm was divided into three stages: the velocity components, the pressure and then the turbulence quantities are calculated using finite volume method discretization of the spatial domain. The Multiphase Segregated Flow (MSF) model was used to model Eulerian Multiphase cases. The term "segregated" refers to the fact that the solution procedure uses the well-known SIMPLE algorithm, which controls the overall solution using separate pressure and velocity solvers, as reported by Patankar and Spalding (2005). The MSF model solves a set of conservation equations for each Eulerian phase present in the simulation. The MSF model is more appropriate for flows that have a constant density. The volume fraction denotes the share of the flow domain that each phase occupies, and each phase has its own velocity and physical properties. To control the calculated results at physical time-steps, the implicit unsteady solver was selected. In the implicit unsteady approach, each physical time-step involves inner iterations to converge the solution for that given instant of time. These inner iterations can be accomplished using spatial integration

schemes, according to CD-Adapco (2014).

In addition, the VOF Waves model was used to simulate the waves where surface gravity acts between air and water. The model can provide flat, first and fifth order waves for various applications. A flat wave was selected for this study to represent the calm water free surface. The Courant-Friedrichs-Lewy (CFL) number relates the cell size to the flow speed and time-step, and must be less than or equal to one for numerical stability (Tezdogan et al., 2015). For the present study, the time-step was selected between 0.005 and 0.01 L/U (where L is waterline length and U is speed), in accordance with the ITTC recommended procedures (ITTC, 2008). The finer the grid and time-step, the better the accuracy at a cost of longer computation time. Reducing the grid size provides a better representation of the model. Conversely, it increases the computation time significantly, and the CPU may not be able to compute the data owing to memory insufficiency.

1. Numerical Ventilation Problem (NVP)

Because of the rotational body motion of the hull, there may be a number of air intakes under the hull that causes the so-called numerical ventilation problem. As the hull speed increases, the amount of air diffusing under the hull increases, because of high trim values. The volume fraction can be deformed under the free surface around the hull. Even with the use of an overset mesh method or other alternate mesh refinement methods around the hull, air still existed under the hull. Federici (2014) mentioned that improvements to the mesh do not address this issue. In most circumstances, this problem may lead to an unwanted drag reduction, of up to 30%.

For a practical application, two approaches can be implemented. The first is multiplying the resultant drag force by the intake percentage of air visualized from the volume fraction of water. For instance, if the visualized diffused air is 15%, multiplying the drag force by 1.15. The second method is to replace the air phase under the hull by the water phase when the solution is converged. The problem will be solved after replacing phases and resuming the calculations for one more time-step. Visualization of the diffused air from the volume fraction graphs can be difficult, therefore phase replacement method with a user-defined function is implemented and recommended. The function replaces the air phase where the volume fraction of air under the hull is below 50%. In extreme conditions when the volume fraction of air is greater than 50%, a new value of air percentage is used from the user-defined function. To reduce or eliminate the numerical ventilation problem, the VOF Phase Replacement model can be used. With this methodology, unwanted air phase is replaced by the water phase in specified regions. Maximum volume fraction can be specified with the method, if appropriate. For a brief step by step explanation, the following list describes the method:

(1) Activate Multiphase Interaction in physics model selection before CFD simulation starts
(2) After numerical solution converged, stop simulation

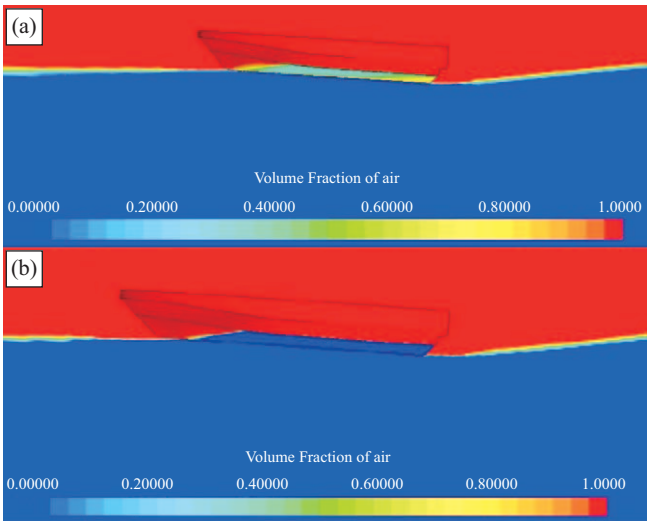

Fig. 8. Planing hull and free surface elevation at Fn = 1.25 (a) numerical ventilation problem under the hull and (b) after replacing the air phase under the hull with the water phase.

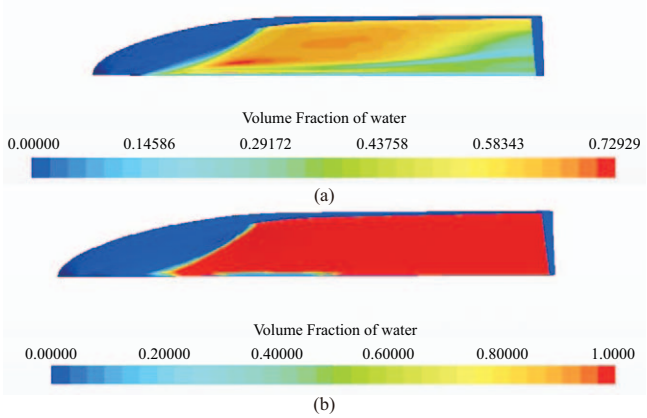

Fig. 9. Planing hull and volume fraction of water at Fn = 1.25 (a) numerical ventilation problem under the hull and (b) after replacing the air phase under the hull with the water phase.

(3) Visualize volume fraction of water graphics
(4) Create a new phase interaction
(5) Select both VOF-VOF Phase Interaction Model and VOF Phase Replacement Model
(6) Use field function for phase replacement
(7) Define Field Function as "${VolumeFractionair} < .50" (This user-defined field function specifies a maximum primary phase volume fraction of 0.5)
(8) For VOF-VOF Phase Interaction, select air for the primary case and select water for the secondary case. This replaces the air phase by water phase
(9) Continue CFD simulation one more time-step
(10) Re-visualize volume fraction

Planing hull free surface elevation and volume fraction of water at Fn = 1.25 are depicted in Fig 8 and Fig 9. In Fig 8(a)

Table 3. Percent errors compared to the experimental results.

Fn	Drag error with NVP	Drag error after phase replacement	C_{TM} error with NVP	C_{TM} error after phase replacement
0.4	-0.88	-0.75	-0.84	-0.77
0.5	-4.84	-2.96	-4.78	-2.90
0.6	-6.59	0.90	-6.56	1.07
0.7	-8.41	-1.40	-8.59	-1.63
0.8	-8.55	-1.10	-8.92	-1.51
0.9	-10.57	0.75	-10.55	0.77
1.0	-16.45	0.84	-16.43	0.83
1.1	-22.25	0.61	-22.36	0.53
1.2	-27.33	2.39	-26.95	2.86

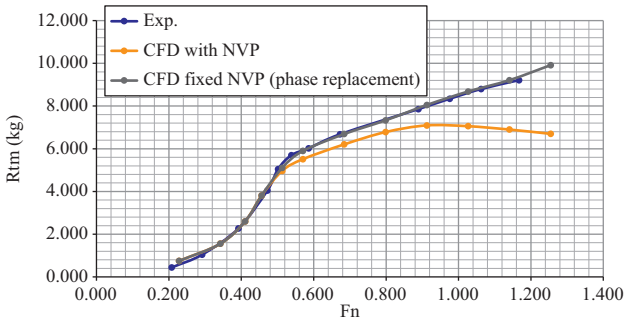

Fig. 10. Comparison of experimental data and simulation results: variation of total resistance R_{TM} in kg for the model scale.

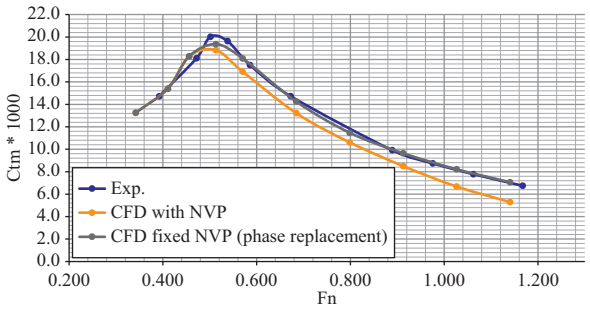

Fig. 12. Comparison of experimental data and simulation results: variation of total resistance coefficient C_{TM}x10^3 for the model scale.

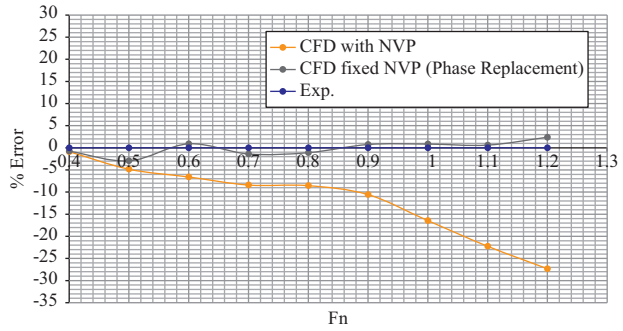

Fig. 11. Percent error of calculated R_{TM} compared to the experimental results.

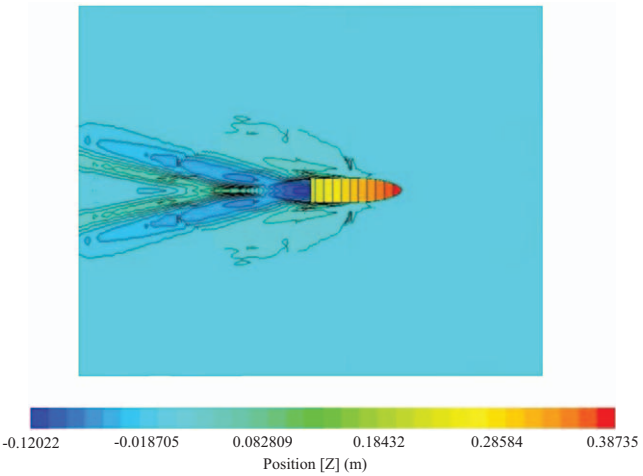

Fig. 13. Wave contours around the model at Fn = 1.25.

and Fig 9(a) the numerical ventilation problem under the hull is observed. In Fig 8(b) and Fig 9(b) it can be seen that after replacing the air phase under the hull by the water phase, the numerical ventilation problem was resolved.

V. RESULTS AND DISCUSSION

Resistance characteristics, trim and sinkage values and full-scale comparison with the sea trial results are presented in this section.

1. Resistance Characteristics

Model scale drag results in kilograms with respect to Froude number are given in Fig. 10, and the percentage error of calculated R_{TM} compared to the experimental results are shown in Fig. 11. The blue line is the experimental result, the orange line is numerical simulation result with the numerical ventilation problem and the gray line is numerical simulation result after phase replacement. The comparison of experimental data and calculated total resistance coefficient ($C_{TM} \times 10^3$) for the model with respect to the Froude number is depicted in Fig. 12. Both drag and C_{TM} percentage errors compared to the experimental results are given in Table 3. As seen from Figs. 10-12, up to Fn = 0.40, experiments and CFD results are nearly identical. Numerical solutions with the numerical ventilation problem

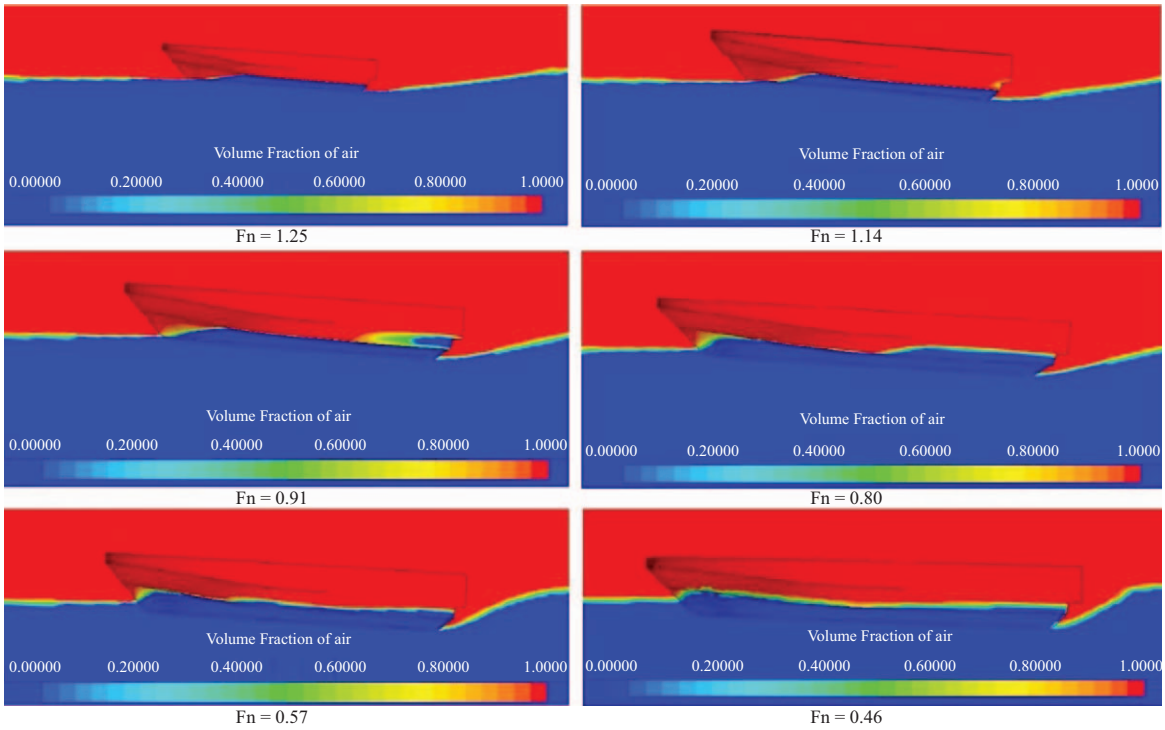

Fig. 14. The model hull and free surface elevation at various Froude numbers.

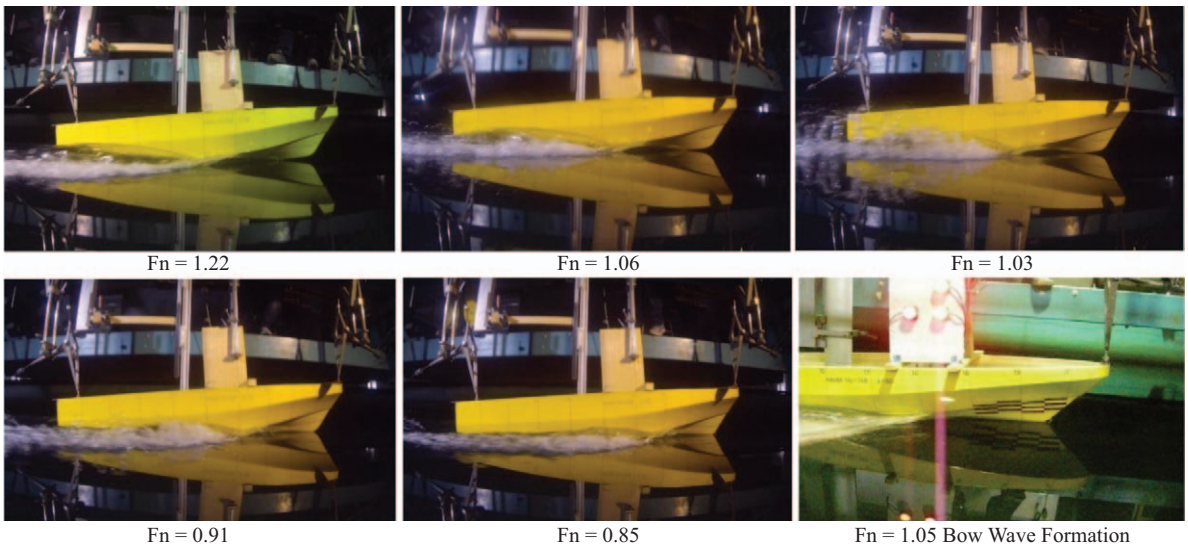

Fig. 15. The model hull at various Froude numbers during model tests.

give erroneous results for Fn greater than 0.40. Subsequently, the boat enters a transient regime, air appears at surface of the hull. CFD calculations with the numerical ventilation problem provide inaccurate results with an erroneous drag reduction of 27% for Fn = 1.2. This is shown in Fig. 11 and Table 3, where the error is 30% at Fn = 1.25. After applying phase replacement, the results show good agreement with the experimental data and the highest error was 2.86%. The model hull generated free surface wave contours at Fn = 1.25, as depicted in Fig. 13. The numerical simulation visualization of the model hull and free surface elevation at various Froude numbers in the planing regime is shown in Fig. 14. Photos from the experiments at various Froude numbers in the planing regime are given in Fig. 15.

Delen and Bal (2015) studied the uncertainty analysis of the resistance tests, which were estimated according to the ITTC (2014) for the same ship model used in the present study. It was reported that the expanded uncertainty value of the resistance test was 0.42% for Fr = 0.90. It was also noted that uncertainty

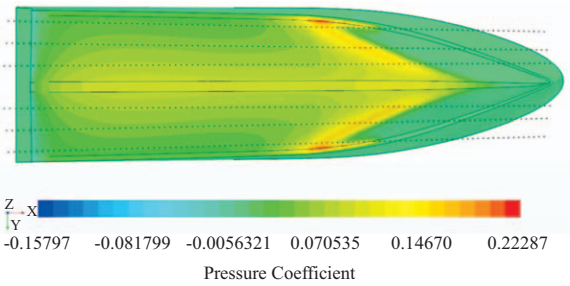

Fig. 16. Pressure coefficient (Cp) distribution near bottom surface at Fn = 1.15.

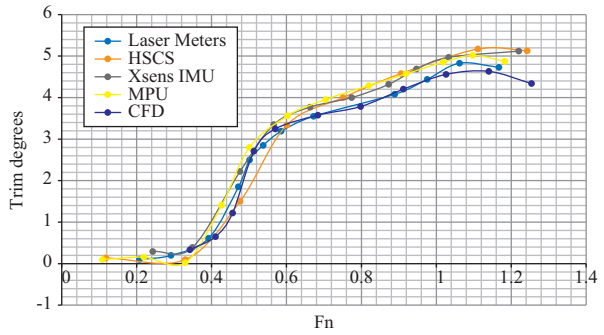

Fig. 17. Comparison of measurements and simulation results: variation of trim angles with respect to Froude numbers.

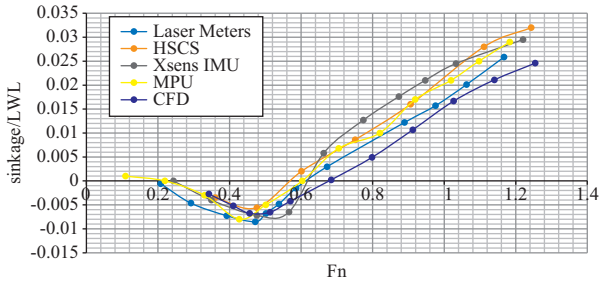

Fig. 18. Comparison of measurements and simulation results: variation of sinkage values with respect to Froude numbers.

sources in the measurement system lost effectiveness when the velocity of the hull was increased.

The computed pressure coefficient (Cp) distribution on the bottom surface is depicted in Fig. 16. It was observed from the computations that the pressure coefficient values peak at the front of the model, and gradually decreased toward the aft of the hull.

2. Trim and Sinkage Characteristics

The results of four different measurement methods for trim and sinkage were compared to numerical simulation results after phase replacement, as shown in Fig. 17 and Fig. 18, respectively. The sinkage values are dimensionless, given as sinkage/L_{WL}. The dark blue line represents the CFD results after phase replacement, the light blue line is the laser distance meter, the orange line is the high-speed camera system (HSCS), the grey line is the Xsens inertial measurement unit (IMU), and the yellow line is the Sparkfun-MPU with Arduino board measurements. The code for conversation of Euler angles from MPU data is given in the Appendix. Both in trim and sinkage comparisons, the CFD results and distance laser meter measurements were very similar. Considering the trim values, all measurement methods and CFD simulations were in good agreement with each other. The poorest measurement method compared to CFD was HSCS with the maximum difference of 15%.

According to the Fig. 18, sinkage values measured by five different methods and simulated by CFD are all within adequate agreement. The negative values in Fig. 18 illustrate sinkage and the positive values illustrate the rising of the model at LCG. Hence, after the model reaches the transient regime, i.e., Fn greater than 0.60, the model begins to raise. For planing high speed hulls, CFD with the phase replacement method and the laser distance meter method are satisfactory for estimating trim and sinkage characteristics.

3. Full-Scale Extrapolation and Sea Trial Results

Because of the nature of the model tests, only the total resistance in model scale was measured, instead of each separate part, which consists of friction and waves. Wave resistance can be scaled, but the friction cannot. Thus, the frictional resistance can be calculated for both model and full-scale using empirical equations. For the present study, the ITTC-78 method was used to extrapolate the drag (ITTC, 2008). The procedure is as follows:

i. Total resistance coefficient for model scale, C_{TM} is calculated for each speed by using:

$$C_{TM} = \frac{R_{TM}}{0.5 \times \rho_M \times V_M{}^2 \times S_M} \tag{10}$$

where R_{TM} is model scale drag, ρ_M is density, V_M is model speed and S_M is wetted surface area.

ii. Frictional resistance coefficient for model scale, C_{FM}, is calculated using ITTC-57 method by using:

$$C_{FM} = \frac{0.075}{(\log_{10} R_{nm} - 2)^2} \tag{11}$$

where Rn_m is model scale Reynolds number.

iii. Residuary resistance coefficient, C_R, which is same for both model scale and full scale is calculated by using:

$$C_R = C_{TM} - C_{FM} \tag{12}$$

iv. Frictional resistance coefficient, C_{Fs}, for full scale is calculated by using:

$$C_{Fs} = \frac{0.075}{(\log_{10} R_{ns} - 2)^2} \tag{13}$$

where R_{ns} is full scale Reynolds number.

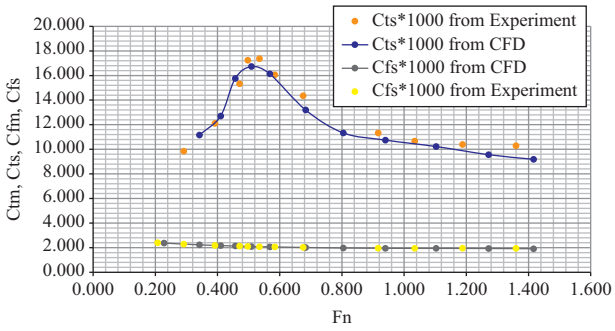

Fig. 19. Full-scale total and frictional resistance coefficients.

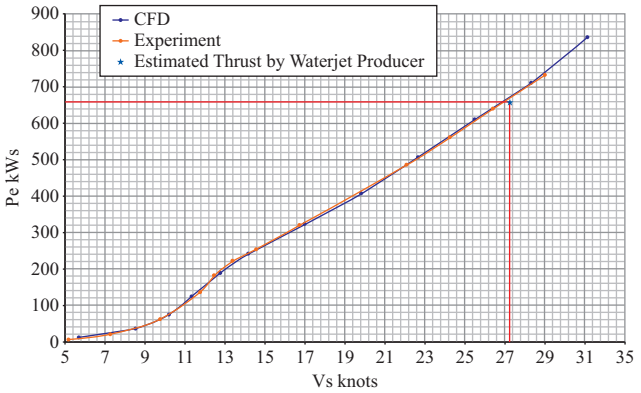

Fig. 20. Comparison of the thrust requirement for the full-scale effective power requirement.

v. Roughness allowance coefficient, C_A, is set to 0.0002 based on the Ata Nutku Ship Model Testing Laboratory's experience.

vi. Air resistance coefficient, C_{AA}, is calculated by using:

$$C_{AA} = \frac{A_{VT}}{1000S} \tag{14}$$

where A_{VT} is surface area projected above the waterline and S is the wetted surface area of the full scale hull.

vii. Total resistance coefficient is calculated by:

$$C_{Ts} = C_{Fs} + C_R + C_A + C_{AA} + C_{Appendages} \tag{15}$$

Since the model is a fast speed hull, form factor analysis was neglected. In the full-scale, the water jet propulsion system was used and there were no appendages, therefore tests were conducted for a bare hull only, and appendage coefficient was neglected. Full-scale total and frictional resistance coefficients with respect to Froude number are given in Fig. 19.

Speed verification for the fully loaded condition was performed and comparison of the thrust requirement for the full-scale effective power with respect to speed is given in Fig. 20. The maximum speed during the sea trial was 27.3 knots and the estimated water jet performance data supplied by the manufacturer was 662 kW. The errors in effective power requirement with the sea trial data are 1.7% and 1.6% according to the CFD results and experimental results, respectively. Hence, the CFD method, model-scale experiments and full-scale trial results are in quite good agreement.

VI. CONCLUSIONS AND FUTURE WORK

In this study, the experimental and numerical methods of resistance prediction of a high speed hull, including the trim and sinkage measurements, were investigated. The model tests were compared to RANS-based simulations using the commercial CFD software STAR-CCM+. The standard k-ε two-equation turbulence model was employed when considering the numerical ventilation problem. It was shown that by resolving the numerical ventilation problem described in this paper, the resistance prediction of high speed hulls can be adequately simulated.

From the experiments and numerical simulations of the high speed model, the following conclusions were reached:

(1) During numerical simulations of high speed crafts, there may be air intakes under the hull causing the numerical ventilation problem (NVP). Mesh improvements may not address the problem. At high speeds, NVP may lead to an erroneous drag reduction of 27%.

(2) To overcome the NVP, two different approaches are employed. The first method was multiplying the resultant drag force value by the intake percentage of air visualized from the volume fraction of water, and the second method is to replacing the air phase under the hull with the water phase. The second approach was more practical and reliable for CFD applications and was used for the results of the present study, as below.
   a. For the numerical solutions at Fn < 0.40, there is no need to employ phase replacement; the drag results are adequate.
   b. For the numerical solutions at Fn > 0.50, the NVP must be resolved by applying phase replacement, and the calculated total resistance shows quite good agreement with the experimental data by a margin of 2.86%.

(3) For the comparison of trim and sinkage measurements, five methods were used: IMU method, low cost MPU method, HSCS, CFD and laser distance meters method. Using the laser distance meter method was reliable and was the easiest way to measure trim and sinkage. After data was collected from the laser meters, it was verified using the hull model's orientation during the tests by photography. Using the laser distance meters method was the best fit to the CFD method.

(4) y^+ values between 40-60 provided more accurate results.

(5) The computations were easily performed on a personal computer by using the standard k-ε turbulence model with phase replacement.

(6) The errors according to the CFD method and experimental results in the effective power requirement were 1.7% and

1.6%, respectively.

(7) The results showed that the ability of the numerical approach within Star-CCM+ for predicting drag around a high speed hull model was quite good if the NVP is resolved. By using more powerful computers, full scale hull forms could be simulated using the same approach.

(8) The EEDI (Energy Efficiency Design Index) is not mandatory for high speed crafts, but it is in place to reduce CO_2 emissions. The calculation of the EEDI coefficient using CFD is a time and cost reduction. Designers can deliver efficient solutions to reduce the EEDI coefficient within the design stage.

It was concluded that the proposed numerical approach can accurately predict the resistance, trim and sinkage calculations of a high speed craft model. For the future work, experimental investigation of high speed crafts in waves is intended. The efficiency of using CFD methods for resistance prediction of a high speed craft in waves will be investigated in future work.

ACKNOWLEDGEMENTS

The authors would like to thank the staff of Ata Nutku Ship Model Testing Laboratory at Istanbul Technical University for their assistance during the experiments and Istanbul Technical University Scientific Research Projects Support Program for partial support of this research through the project ITU-BAP-38875. The authors also would like to thank "Loça Mühendislik" Ship Design Company for their support and for access to the full-scale trial data.

APPENDIX

An Arduino code that allows printing of the raw accelerometer, gyro, and magnetometer data is given below.

```
#include <Wire.h>
#include "I2Cdev.h"
#include "MPU9150Lib.h"
#include "CalLib.h"
#include <dmpKey.h>
#include <dmpmap.h>
#include <inv_mpu.h>
#include <inv_mpu_dmp_motion_driver.h>
#include <EEPROM.h>

MPU9150Lib MPU;                                  // the MPU object

//  MPU_UPDATE_RATE defines the rate (in Hz) at which the MPU updates the sensor data and DMP output

#define MPU_UPDATE_RATE (8)

//  SERIAL_PORT_SPEED defines the speed to use for the debug serial port

#define  SERIAL_PORT_SPEED  9600

void setup()
{
   Serial.begin(SERIAL_PORT_SPEED);
   Serial.println("Arduino9150 starting");
   Wire.begin();
   MPU.init(MPU_UPDATE_RATE);                    // start the MPU
}

void loop()
{
  if (MPU.read()) {                              // get the latest data
//  MPU.printQuaternion(MPU.m_rawQuaternion);          // print the raw quaternion from the dmp
//  MPU.printVector(MPU.m_rawMag);                 // print the raw mag data
//  MPU.printVector(MPU.m_rawAccel);               // print the raw accel data
```

```
//  MPU.printAngles(MPU.m_dmpEulerPose);          // the Euler angles from the dmp quaternion
//  MPU.printVector(MPU.m_calAccel);              // print the calibrated accel data
//  MPU.printVector(MPU.m_calMag);                // print the calibrated mag data
    MPU.printAngles(MPU.m_fusedEulerPose);        // print the output of the data fusion
    Serial.println();
  }
}
```

REFERENCES

Avci, A. G. and B. Barlas (2015). A Practical Application for Trim and Sinkage Measurements for High Speed Marine Vessels by Using an Inertial Measurement Unit and an Arduino Board. 4th International Conference on Advanced Model Measurement Technology for the Maritime Industry, Istanbul.

Brizzolara, S., F. Serra (2011). Accuracy of CFD codes in the prediction of planing surfaces hydrodynamic characteristics. 2nd International Conference on Marine Research and Transportation, Italy.

CD-Adapco (2014). User guide STAR-CCM+ Version 9.0.2.

Cerka, J., R. Mickeviciene, Z. Asmontas, L. Norkevicius, T. Zapnickas, V. Djackov and P. Zhou (2017). Optimization of the Research Vessel Hull Form by Using Numerical Simulation. Ocean Engineering 139, 33-38.

Clement, E. P. and D. Blount (1963). Resistance Tests of Systematic Series of Planing Hull Forms. SNAME Transaction, 71, 491-579.

Delen, C. and Ş. Bal (2015). Uncertainty analysis of resistance tests in Ata Nutku Ship model testing Laboratory of Istanbul Technical University. Journal of Maritime and Marine Sciences, 1(2 (2015)), 8-27.

Dixit, S. A. and O. N. Ramesh (2009). Determination of skin friction in strong pressure-gradient equilibrium and near equilibrium turbulent boundary layers. Experiment Fluids 47(6), 1045-1058.

Faltinsen, O. M. (2006). Hydrodynamics of High-Speed Marine Vehicles, Cambridge University Press.

Federici, A. (2014). Design and analysis of non-conventional hybrid high speed hulls with hydrofoils by CFD methods, University of Genoa, Genoa.

Ghassemi, H. and M. Ghiasi (2008). A combined method for the hydrodynamic characteristics of planing crafts. Ocean Engineering 35, 310-322.

ITTC (2008). Testing and extrapolation methods high speed marine vehicles, In: Specialist Committee on Powering Performance Prediction 25th ITTC. Available from: (http://ittc.info/media/1279/75-02-05-01.pdf) (accessed 08.06.17).

ITTC, 2014. General guideline for uncertainty analysis in resistance tests (7.5-02-02-02). Available from: (https://ittc.info/media/4056/75-02-02-021.pdf) (accessed 11.04.18).

Kim, D. J., S. Y. Kim, Y. J. You, K. P. Rhee, S. H. Kim and Y. G. Kim (2013). Design of high-speed planing hulls for the improvement of resistance and seakeeping performance. International Journal of Naval Architecture and Ocean Engineering 5, 161-177.

Mousaviraad, S. M., Z. Wang and F. Stern (2015). URANS studies of hydrodynamic performance and slamming loads on high-speed planing hulls in calm water and waves for deep and shallow conditions. Applied Ocean Research 51, 222-240.

Panahani, R., E. Jahanbakhsh and M. S. Seif (2009). Towards simulation of 3D nonlinear high-speed vessels motion. Ocean Engineering 36, 256-265.

Patankar, S. V. and D. B. Spalding (2005). A calculation procedure for heat, mass and momentum transfer in three-dimensional parabolic flows. Int. J. Heat Mass Transfer 15(2), 1787-1806.

Santoro, N., E. Begovic, C. Bertorello, A. Bove, S. De Rosa and F. Franco (2014). Experimental study of the hydrodynamic loads on high speed planing craft. Procedia Engineering 88,186-193.

Savitsky, D. (1964). Hydrodynamic design of planing hulls. Marine Technology 1(1), 71-95.

Stern, F., Z. Wang, J. Yang, H. Sadat-Hosseini, M. Mousaviraad, S. Bhushan, M. Diez, S. H. Yoon, P. C. Wu, S. M. Yeon and T. Dogan (2015). Recent Progress in CFD for naval architecture and ocean engineering. Journal of Hydrodynamics Ser. B, 27, 1-23.

Sukas, O. F., O. K. Kinaci, F. Cakici and M. K. Gokce (2017). Hydrodynamic assessment of planing hulls using overset grids. Applied Ocean Research 65, 35-46.

Su, Y., S. Wang, H. Shen and X. Du (2014). Numerical and experimental analyses of hydrodynamic performance of a channel type planing trimaran. Journal of Hydrodynamics Ser. B, 26,549-557.

Tezdogan, T., Y. K. Demirel, P. Kellett, M. Khorasanchi, A. Incecik and O. Turan (2015). Full-scale unsteady RANS CFD simulations of ship behaviour and performance in head seas due to slow steaming. Ocean Engineering 97, 186-206.

Yousefi, R., R. Shaafaghat and M. Shakeri (2013). Hydrodynamic analysis techniques for high-speed planing hulls. Applied Ocean Research 42, 105-113.